J. Fluid Mech. (2024), *vol*. 1000, A38, doi:10.1017/jfm.2024.1030

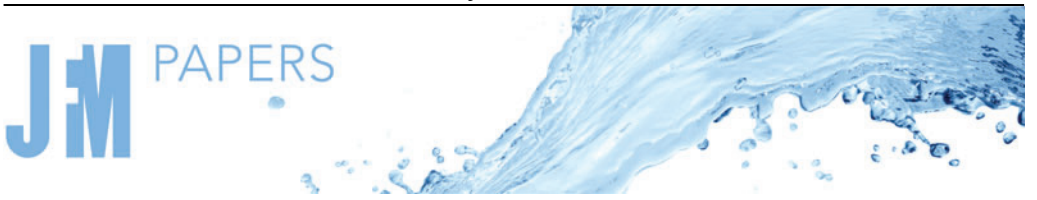

Existence of Bolgiano–Obukhov scaling in the bottom ocean?

Peng-Qi Huang[1], Shuang-Xi Guo[1,4,†], Sheng-Qi Zhou[1,4,†], Xian-Rong Cen[2], Ling Qu[3], Ming-Quan Zhu[1,4] and Yuan-Zheng Lu[1]

[1]State Key Laboratory of Tropical Oceanography, South China Sea Institute of Oceanology, Chinese Academy of Sciences, Guangzhou 510301, PR China

[2]School of Industrial Design and Ceramic Art, Foshan University, Foshan 528000, PR China

[3]Geophysical Exploration Brigade of Hubei Geological Bureau, Wuhan 430056, PR China

[4]University of Chinese Academy of Sciences, Beijing 100049, PR China

(Received 25 March 2024; revised 23 September 2024; accepted 21 October 2024)

The seminal Bolgiano–Obukhov (BO) theory established the fundamental framework for turbulent mixing and energy transfer in stably stratified fluids. However, the presence of BO scalings remains debatable despite their being observed in stably stratified atmospheric layers and convective turbulence. In this study, we performed precise temperature measurements with 51 high-resolution loggers above the seafloor for 46 h on the continental shelf of the northern South China Sea. The temperature observation exhibits three layers with increasing distance from the seafloor: the bottom mixed layer (BML), the mixing zone and the internal wave zone. A BO-like scaling $\alpha = -1.34 \pm 0.10$ is observed in the temperature spectrum when the BML is in a weakly stable stratified ($N \sim 0.0018$ rad s^{-1}) and strongly sheared ($Ri \sim 0.0027$) condition, whereas in the unstably stratified convective turbulence of the BML, the scaling $\alpha = -1.76 \pm 0.10$ clearly deviated from the BO theory but approached the classical $-5/3$ scaling in isotropic turbulence. This suggests that the convective turbulence is not the promise of BO scaling. In the mixing zone, where internal waves alternately interact with the BML, the scaling follows the Kolmogorov scaling. In the internal wave zone, the scaling $\alpha = -2.12 \pm 0.15$ is observed in the turbulence range and possible mechanisms are provided.

Key words: turbulent convection, stratified turbulence, boundary layer structure

1. Introduction

Oceanic turbulent mixing plays a crucial role in controlling the meridional overturning circulation and heat budget, and subsequently in shaping global climate states

† Email addresses for correspondence: sxguo@scsio.ac.cn, sqzhou@scsio.ac.cn

(Ganachaud & Wunsch 2000; Wunsch & Ferrari 2004; Hieronymus *et al.* 2019). Numerous efforts have been made to comprehend the connections between large-scale processes and small-scale turbulence in oceans. Compared with the stratified atmosphere, where atmospheric turbulence has been studied through spectral and structure–function analyses for decades (Gage 1985; Frehlich & Sharman 2010), in the ocean, more attention has been focused on mesoscale and submesoscale turbulence and internal wave mixing (e.g. Meredith & Garabato (2021) and references therein), while less attention has been paid to small-scale turbulence, especially to the cascade scaling behaviours in various turbulent regimes.

The ocean is generally considered to be a stratified fluid. In stably stratified fluids, Bolgiano (1959) and Obukhov (1959) (BO) proposed the 'buoyant subrange' in the spectrum, where turbulence energy is suppressed by negative buoyancy forces associated with a hydrostatically stable environment and the buoyant flux exceeds the kinetic energy flux. Based on dimensional analysis, the kinetic energy spectrum $E_u(k)$ and the thermal energy spectrum $E_\theta(k)$ were predicted to scale as $k^{-11/5}$ and $k^{-7/5}$, respectively, where k is the wavenumber. However, this BO scaling has rarely been observed in the ocean. Instead, observations of vertical wavenumber spectra of temperature in the open ocean (Gregg 1977; van Haren & Gostiaux 2009) and composite spectrum of velocity shear (Gargett *et al.* 1981) showed the spectrum to fall as k^{-3}, consistent with the theoretical prediction by Monin (1962) and Lumley (1964). More observations have found transition of the energy spectrum from k^{-3} to $k^{-5/3}$, representing the scaling law in homogeneous isotropic turbulence (Kolmogorov 1941), for high-Reynolds-number turbulence in the interior ocean (Ewart 1976; Gargett, Osborn & Nasmyth 1984; Holbrook & Fer 2005; Klymak & Moum 2007).

Comparatively, the BO scaling has been observed in the stably stratified atmospheric surface layer (Chiba 1989), lower stratosphere (Cot & Barat 1989), troposphere (Lazarev *et al.* 1994), lower stratosphere and upper troposphere (Werne & Fritts 2000; Wroblewski *et al.* 2010). However, different results have also been obtained in other works. The BO scaling has not been observed in weak or strong stratification at a height of 2 m over flat grassland (Okamoto & Webb 1970). Turbulent wind spectra have scalings from 11/5 to 3 for stable stratification and are closer to the Kolmogorov theory for neutral stratification at the surface atmosphere layer (Myrup 1969). The change from the BO to Kolmogorov scalings can be observed for different scale ranges in temperature measurements at altitudes of approximately 10 km (Wroblewski *et al.* 2007). Although the BO scaling has also been observed in unstably stratified convective turbulence in laboratory experiments (Wu *et al.* 1990; Zhou & Xia 2001) and theoretical arguments (Yakhot 1992; Ching 2014), its existence is still debatable (for a review, see Lohse & Xia (2010)).

Some numerical simulations report inconsistent views regarding stably stratified and convective turbulence as well. In certain simulations, the velocity spectrum follows the BO scaling in strongly stratified or moderately stratified regimes, while it follows the Kolmogorov scaling for weak stratification (Kumar, Chatterjee & Verma 2014; Alexakis & Biferale 2018; Alam, Guha & Verma 2019; Basu & Bhattacharjee 2019; Agrawal & Chandy 2021). For very weak and/or strong stratifications, where the buoyancy forces are relatively irrelevant or the flow fields are effectively two-dimensionalized, the kinetic energy spectra show the Kolmogorov scaling (Basu & Bhattacharjee 2019; Agrawal & Chandy 2021). In a cascade model simulation, Shestakov, Stepanov & Frick (2017) believe that the BO regime exists only when the work of the buoyancy force and the nonlinear energy transfer over the spectrum are balanced within a certain range of scales, which is not satisfied either in convective turbulence or in turbulence with stable stratification.

According to the literature review mentioned above, it appears that the BO scaling may exist in stratified fluids and potentially in convective turbulence, which motivates further exploration of this issue in highly turbulent oceanic environments. In addition, recent *in situ* observations have revealed BO-like scaling in the deep ocean (near bottom) of the Rockall Canyon (van Haren *et al.* 2024), the Gulf of Mexico (Polzin *et al.* 2021) and other regions (e.g. van Haren & Dijkstra 2021; van Haren & Bosveld 2022). These studies suggest that the $-7/5$ scaling in the temperature spectrum is indicative of buoyancy-driven convective turbulence (van Haren *et al.* 2024), which needs further clarification due to its importance in abyssal ocean exploration. The South China Sea (SCS), known as the most active marginal sea, exhibits significantly enhanced mixing with turbulence levels two orders of magnitude higher than those in the Pacific Ocean (Tian, Yang & Zhao 2009; Yang *et al.* 2016). The intense mixing in the SCS is primarily driven by internal waves, which originate in the Luzon Strait and propagate westward into the continental shelf and deep basin (Zhao 2014; Alford *et al.* 2015). The Dongsha Plateau, situated on the northern continental shelf of the SCS, lies directly in the path of these internal waves, where a potential maximum balance between wave energy and instability may exist (St. Laurent *et al.* 2011). Recent observations have indicated the alternative occurrence of stratified turbulence and convective turbulence in the bottom ocean of the Dongsha Plateau (Qu *et al.* 2021). This unique environment provides an ideal opportunity to explore the turbulent energy cascading in different flow and stratification regimes within the ocean.

In this study, we examine the existence of BO scaling in the bottom ocean near Dongsha Atoll at a depth of 278 m on the continental shelf. The paper is organized as follows. In § 2, we present the hydrographic data and data processing. Then we describe the water characteristics and temperature spectrum scalings in § 3, discuss the BO-like scaling in the convective turbulence and stratified turbulence of different stratifications in § 4 and summarize the main points in § 5.

2. Hydrographic data and data processing

2.1. *Hydrographic data*

Between 15 April and 21 May 2020, a comprehensive oceanographic survey was undertaken in the SCS using the Jiageng R/V. As part of this survey, a 46-hour experiment was carried out starting at 17:44 local time (LT) on 15 May at a site northwest of Dongsha Atoll (21.24° N, 116.07° E) with a water depth of 278 m (figure 1*a*). The topographic slope angle at this location is 0.61° based on the GEBCO topography dataset. In the experiment, an instrumented full-depth mooring was deployed, equipped with a tripod lander frame at the bottom (figure 1*b*). The mooring set-up included various sensors and instruments: 25 SBE56 temperature loggers (Sea-bird Electronics), 76 ONT18S temperature loggers (Ocean Net Technology Co. Ltd), three Infinity-CT (JFE Advantech), one CTD and two RBR-TD (RBR), one current meter (SeaGuard) and one ADCP (300 kHz, Teledyne RDI). The tripod lander frame had a height of 2.2 m. On one vertical arm of the frame, 22 ONT18S temperature loggers were mounted with equal spacing of 0.1 m from the lowest one, which was located 0.01 m above the bottom ($Dab = 0.01$ m). The RBR-CTD was mounted on a different arm at $Dab = 1.20$ m. Moving upward from the top of the frame to the sea surface, the temperature loggers were arranged as follows: 10 ONT18S temperature loggers with a vertical spacing of 1 m, 36 ONT18S temperature loggers with a spacing of 2 m, 20 SBE56 temperature loggers with a spacing of 5 m and five SBE56 temperature loggers with a spacing of 20 m. Two RBR-TD sensors were mounted at $Dab = 125.6$ and 266 m and three Infinity-CT were mounted at $Dab = 22$, 55 and 125 m. The ONT18S

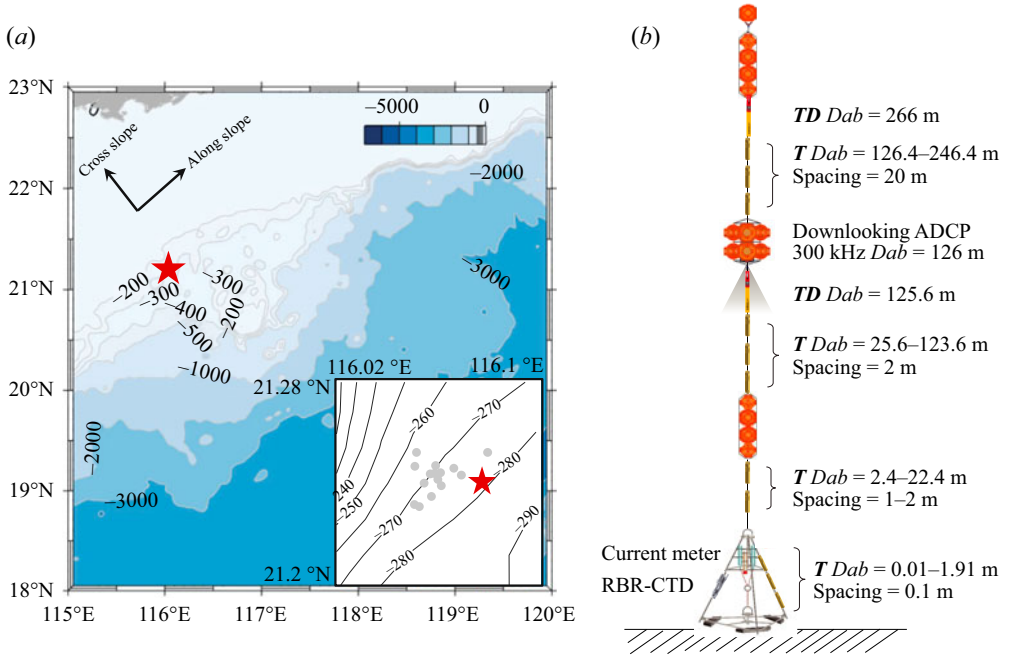

Figure 1. (*a*) Bathymetric map of the northeastern SCS extrapolated from GEBCO gridded bathymetry data. The tripod mooring location is represented by the red star. The coordinates (x, y) are defined as x along the slope direction (positive to the northeast) and y in the cross-slope direction (positive onshore). The inset shows a zoomed-in view of the map near the mooring station. The grey circles indicate the CTD stations. (*b*) Schematic diagram illustrating the configuration of the tripod mooring.

temperature logger was used for its small time constant of 0.3 s and a low noise level of 1×10^{-4} °C. It was set to sample at a rate of 16 Hz to capture the small-scale water structures. The sampling rates for RBR-CTD, RBR-TD, SBE56 and Infinity-CT sensors were set at 16, 2, 1 and 1/60 Hz, respectively. Additionally, a down-looking 300 kHz ADCP was mounted at a depth of approximately $Dab = 126$ m. It was programmed to sample at an interval of 60 s with a bin size of 4 m. In the present study, the focus was on the turbulent cascading behaviours within the bottom 80 m, in which the temperature was precisely recorded using 51 ONT18S temperature loggers.

Meanwhile, a CTD rosette cast was performed every 3 h at the mooring site, reaching a maximum depth of around 258 m, approximately 20 m above the ocean bottom. The rosette included a 300 kHz lowered acoustic Doppler current profiler (LADCP; Teledyne RDI) and an SBE911 Plus CTD to measure the flow and water properties such as velocity, temperature, salinity and pressure. The CTD collected data at a sampling rate of 24 Hz. The LADCP was configured with 20 bins of bin size 8 m to capture the flow characteristics. Due to the influence of wind and surface ocean currents, the vessel experienced frequent drift, but it was restored to the set location within a range of approximately 2.5 km, as shown in the inset of figure 1(*a*). Additionally, a vertical microstructure profiler (VMP250, Rockland Scientific) was deployed every hour from 19:00 LT on 15 May to 00:30 LT on 18 May with a sampling rate of 512 Hz, measuring the turbulent kinetic energy dissipation rate ε. To avoid potential damage from the complex topography, the VMP250 approached depths ranging from 5 to 50 m above the seafloor during each deployment.

2.2. *Data processing*

In order to precisely measure the fine thermal variations in the bottom ocean, the ONT18S temperature loggers underwent laboratory calibration prior to field deployment. Additionally, the ONS18S temperature loggers were cross-calibrated using the data of RBR-CTD at $Dab = 1.2$ m. As a result, these calibration procedures improved the temperature loggers' precision of 1×10^{-3} and resolution of 1×10^{-4} °C.

For further analysis, it is necessary to convert the *in situ* temperature T to potential temperature θ and potential density σ_0. This conversion relies on the relationship obtained from the full-depth temperature and salinity profiles with the SBE911 Plus CTD. As shown in figure 2(*a*), the potential temperature, θ, appears to be proportional to the *in situ* temperature T. Figure 2(*b*) shows that the potential density, σ_0, decreases as the *in situ* temperature, T, increases, but the relationship is nonlinear. The best-fit equations are given by

$$\theta = 1.002\,T - 0.0616, \tag{2.1}$$

$$\sigma_0 = 4.06 \times 10^{-4}\,T^3 - 0.0315\,T^2 + 0.486\,T + 24.08. \tag{2.2}$$

The water stratification can be described by the buoyancy frequency $N = [-(g/\rho_0) \times (\mathrm{d}\sigma_0/\mathrm{d}z)]^{1/2}$, where g is the gravitational acceleration and $\rho_0 = 1024.9$ kg m^{-3} is the reference density. Figure 2(*c*) shows the nominal profile of N. The thermocline occurs in the upper 150 m, which serves as the main passage channel of internal waves because of the strong stratification larger than 0.01 rad s^{-1}. Then, N gradually diminishes with increasing depth. In the depth range below 200 m (approximately 80 m above the bottom), N decreases from 7×10^{-3} to 3×10^{-3} rad s^{-1}.

In stably stratified shear flows, the relative strength of the density and velocity gradients is assessed using the Richardson number, Ri. This dimensionless parameter is defined as $Ri = N^2/S^2$ with $S = \partial U/\partial z$ being the shear term. The Richardson number Ri quantifies the balance between the suppression of turbulence due to buoyancy and the generation of turbulence due to shear. The velocity profiles obtained from the LADCP measurements can be used to determine S and subsequently calculate Ri. Figure 2(*d*) illustrates the profiles of Ri. Excluding the surface mixed layer, the nominal Ri is of the order of 1 and gradually decreases with increasing depth, ranging between 0.1 and 10. Within the depth range of 40 m above the ocean bottom, Ri is consistently below 0.25, which is considered the critical value for the onset of shear instability (Osborn 1980).

3. Results

3.1. *Multilayer structures in the bottom ocean*

In the observation region, internal waves are the primary dynamic activities responsible for the enhanced turbulent mixing (St. Laurent *et al.* 2011; Alford *et al.* 2015). Figure 3(*a*) shows the temperature variability of the bottom ocean. There are frequent downward thermal bursts with vertical excursions of up to 50 m, which indicate the presence of high-frequency internal waves persisting for durations ranging from a few minutes to several hours. The variation of the buoyancy frequency (figure 3*b*) provides a clearer demonstration of trough structures of high-frequency internal waves. In addition, the bottom water can be divided into three distinct layers characterized by different stratifications. In the depth range above $Dab = 40$ m, the water stratification is primarily modulated by the intense internal waves. This region is referred to as the internal wave zone. Near the ocean bottom, there is an obvious stratified belt of approximately

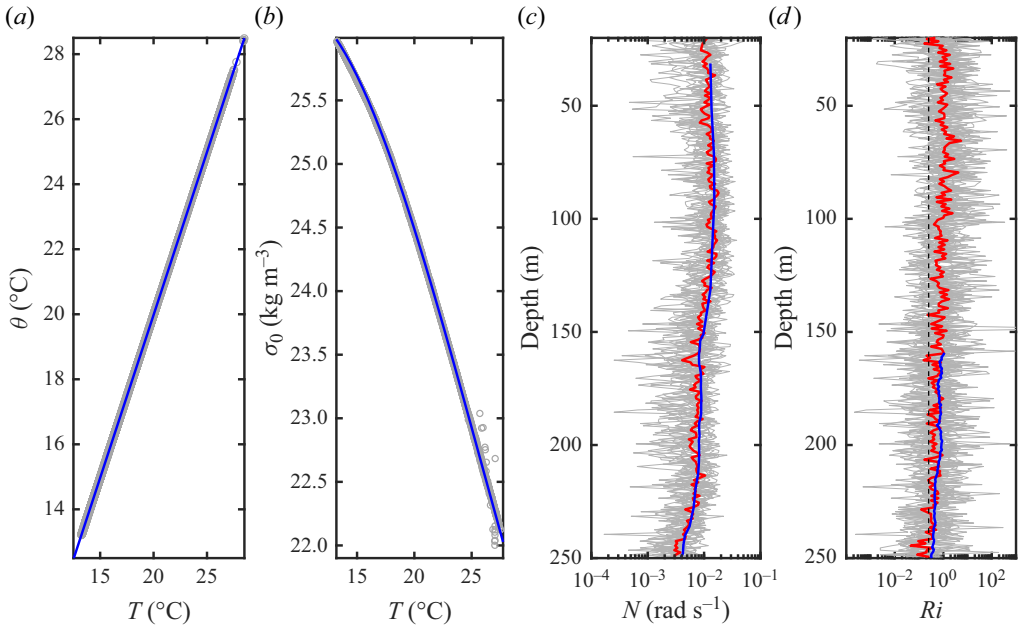

Figure 2. (*a*) Potential temperature, θ, and (*b*) potential density, σ_0, as a function of *in situ* temperature, T, of all 18 profiles measured with the SBE911 Plus CTD at the mooring site. In (*a*,*b*), the blue lines represent the polynomial fits (equations (2.1) and (2.2)). Based on the CTD and LADCP data, the profiles of (*c*) the buoyancy frequency, N, and (*d*) the Richardson number, Ri, are indicated with grey lines, and their corresponding median values are shown as red lines. The median values of N and Ri inferred from the mooring data are shown as blue lines. The dashed line marks $Ri = 0.25$.

0.006 rad s^{-1} around $Dab \sim 10$ m. Below this belt lies the bottom boundary layer, known as the bottom mixed layer (BML), which exhibits a lower level of stratification. Between a depth of $Dab = 40$ m and the bottom stratified belt, the water stratification appears to vary in a diurnal cycle. In contrast to the relatively strong stratification of approximately 0.007 rad s^{-1} in the internal wave zone, it is as weak as 0.0024 rad s^{-1} in the time intervals of day [136.6, 137.3] and day [137.7, 138.4], and becomes double around 0.0047 rad s^{-1} during day [137.3, 137.7] and day [138.4, 138.7]. This depth range is referred to as the mixing zone because the stratification is alternately modulated by the interactions between the overlying internal waves and the BML.

The BML is a quasi-homogeneous layer in the ocean characterized by uniform temperature, salinity, density and other properties (Weatherly & Martin 1978; Shimizu 2010; Trowbridge & Lentz 2018; Huang *et al.* 2019, 2021). By analysing the vertical temperature profiles detected from the densely distributed thermistors, we determine the thickness of the BML, H_{BML}, and examine its evolution. To accurately determine the BML from less fluctuating profiles, the temperature is averaged every 60 s. The thickness H_{BML} is computed as the distance from the bottom to the point where the potential temperature changes by 0.02 °C. In the observation period, H_{BML} exhibits high intermittency, ranging from 0.8 to 10.4 m, with an average of approximately 4.1 m. This confirms the persistent nature of the BML above the seafloor, consistent with previous reports (Qu *et al.* 2021). Within the BML, the buoyancy frequency averages around 0.0018 rad s^{-1}, ranging from unstable stratification to 0.005 rad s^{-1}.

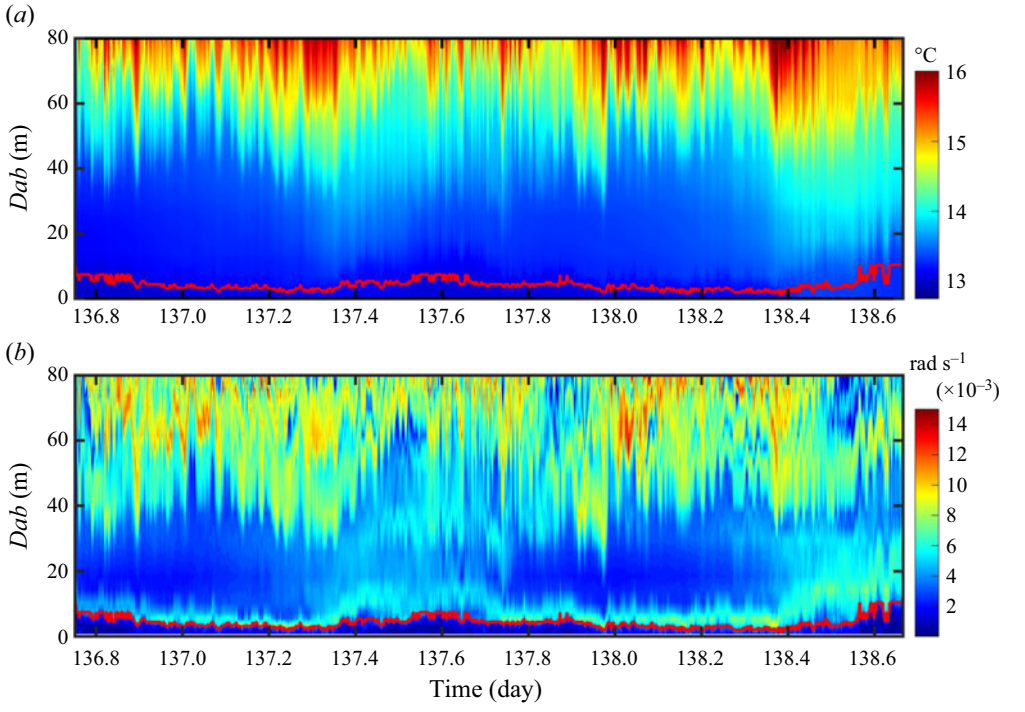

Figure 3. (*a*) Time–depth potential temperature θ variability in the bottom ocean ($Dab = [0, 80]$ m) using 51 thermistors at a sampling rate of 16 Hz. (*b*) The inferred buoyancy frequency N in the bottom ocean. The red lines denote the upper boundary of the BML.

3.2. *Scaling behaviour in the temperature spectrum*

The precise temperature measurements available allow us to examine the scaling behaviour in turbulent oceanic conditions. The smallest turbulent scale can be assessed using the Kolmogorov time scale, defined as $\tau_\eta = \sqrt{\nu/\varepsilon}$, where ν is the kinematic viscosity (Kolmogorov 1941). For typical values on the shelf of the northern SCS, $\nu \sim 10^{-6}$ m^2 s^{-1} and $\varepsilon \sim 10^{-8}$ m^2 s^{-3} (St. Laurent *et al.* 2011; Qu *et al.* 2021), the estimated Kolmogorov time is approximately $\tau_\eta \sim 10$ s. Thus, all possible turbulent states, including the so-called inertial range, can be well resolved here (Frisch 1995).

The temperature spectra in three layers, i.e. the BML, the mixing zone and the internal wave zone, are individually examined to learn the influences of different dynamic processes. To ensure sufficient statistics over a broad frequency range, all temperature data recorded within the same zone are depth-averaged, resulting in less fluctuating spectra. Figure 4 illustrates the power spectra for each layer. Within the BML, the temperature spectrum E_θ exhibits a scaling behaviour in the frequency range $\langle N_{BML}\rangle < \omega < 0.3$ rad s^{-1}, where $\langle N_{BML}\rangle$ is the averaged buoyancy frequency of $\sim$0.002 rad s^{-1}. The best data fitting yields a scaling exponent of $\alpha = -1.34 \pm 0.07$. This scaling exponent is in close agreement with the theoretical prediction of BO scaling, $-7/5$ (Bolgiano 1959; Obukhov 1959). Similar scaling laws have also been observed in recent studies of van Haren's group in the deep alpine Lake Garda (van Haren & Dijkstra 2021), the deep slope at Mount Josephine in the northeastern Atlantic (van Haren 2022) and the deep western Mediterranean (van Haren 2023).

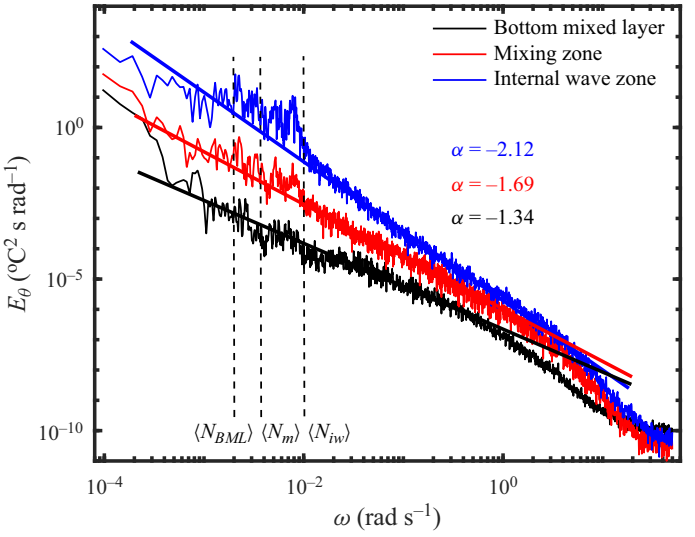

Figure 4. The averaged temperature spectra E_θ in the internal wave zone ($Dab = [40, 80]$ m, blue), mixing zone ($Dab = [10, 40]$ m, red) and BML ($Dab = [0, H_{BML}]$, black), with the corresponding fitted power scalings of -1.34, -1.69 and -2.12. The vertical dashed lines indicate the nominal buoyancy frequency in the internal wave zone $\langle N_{iw}\rangle$, mixing zone $\langle N_m\rangle$ and BML $\langle N_{BML}\rangle$.

In the mixing zone, the temperature spectrum shows fluctuations at frequencies below the averaged buoyancy frequency of $\langle N_m\rangle \sim 0.003$ rad s^{-1}, likely attributed to intermittent influences of internal waves. In the range $0.01 < \omega < 0.5$ rad s^{-1}, the spectrum exhibits a consistent scaling behaviour, with the best-fitted scaling exponent of $\alpha = -1.69 \pm 0.07$. This scaling exponent is remarkably close to Kolmogorov's prediction $(-5/3)$ for isotropic turbulence. The presence of the classical Kolmogorov scaling has been extensively observed in the ocean, as reported in Moum (2015), Becherer & Moum (2017), Ewart (1976), Klymak & Moum (2007) and Holbrook & Fer (2005).

According to the classical BO phenomenology, the Bolgiano scale l_B is defined as $l_B = N^{-3/2}\varepsilon^{5/4}\chi^{-3/4}$, where ε is the energy dissipation rate and χ is the temperature dissipation rate. The spectrum will be Kolmogorov-like for the length scale $l < l_B$ and BO-like for $l > l_B$. Here, the observation of Bolgiano scaling in the BML and Kolmogorov scaling in the mixing zone suggests that l_B should be small near the ocean bottom and increase on moving away from the bottom when the BO theory is applicable. There has been little work on l_B around the boundary layer in stratified turbulent flow. However, numerical simulations in turbulent thermal convections have shown a distribution similar to the present observation (Calzavarini, Toschi & Tripiccione 2002; Kunnen *et al.* 2008). In these studies, it is found that l_B is small near the boundary and increases gradually when far from the boundary, corresponding to a transition from a BO-dominated regime near the wall to a Kolmogorov regime moving away from the boundary (Calzavarini *et al.* 2002).

In the internal wave zone, the water is more stratified with averaged buoyancy frequency $\langle N_{iw}\rangle \sim 0.01$ rad s^{-1}. The clear single scaling shifts to a higher-frequency range of $0.02 < \omega < 1$ rad s^{-1}, with the best-fitted scaling exponent of $\alpha = -2.12 \pm 0.15$. The presence of a -2 scaling in oceanography primarily reflects the canonical ocean-interior saturated internal wave, which occurs between the inertial frequency f and the buoyancy frequency N. This frequency range is typically much smaller than the turbulent inertial

range (Garrett & Munk 1972). Phillips (1971) proposed that continuously breaking internal waves would leave a trail of locally mixed fluid in the travelling waves, and the fine structures are advected by large-scale internal waves, where the advection process leads to broadband contamination of Eulerian time series, resulting in a -2 scaling. A similar -2 scaling was also observed by van Haren (2023) in the turbulence regime at approximately 100 m above the seafloor in the western Mediterranean, and they proposed that nonlinear interactions in internal waves may transfer their energy into irreversible turbulence, this spectral property being related to the chaos theory of Brownian noise (Schuster & Just 2006).

4. Discussion

Extensive observations of the Kolmogorov scaling have been documented in the velocity or temperature spectra of the oceanic bottom boundary layer across various environments, including bays (Gross & Nowell 1985), tidal channels (Lien & Sanford 2004), continental shelves (Chriss & Caldwell 1984) and deep ocean (van Haren & Gostiaux 2009). Recent studies by van Haren & Dijkstra (2021) and van Haren (2022, 2023) have also reported the presence of BO scaling in the bottom ocean through precise temperature measurements, which is proposed to be associated with active scalar buoyancy-driven turbulent convection.

The applicability of the BO phenomenology in buoyancy-driven turbulent convection has sparked controversy. While some studies observed BO scaling, others report a Kolmogorov-like spectrum (e.g. Ahlers, Grossmann & Lohse (2009), Lohse & Xia (2010) and references therein). Recent arguments challenge the validity of the BO theory, suggesting that the total energy cascade cannot remain balanced under unstable stratification, contradicting the premise of BO theory (Kerr 1996; Kumar *et al.* 2014; Verma, Kumar & Pandey 2017).

Within the BML, the water experiences alternating weak and unstable stratification. Figure 5(*a*) shows the square of the buoyancy frequency N^2 within the BML, indicating convective instability during two time periods (day [137.44, 137.58] and day [138.57, 138.67]), where N^2 is slightly less than zero. The convective process can be quantified using the Rayleigh number $Ra = g\Delta\sigma_{max}H_{BML}^3/(\rho_0\nu\kappa_\theta)$, where $\Delta\sigma_{max} = \alpha'\Delta\theta_{max}$ is the maximum negative density anomaly relative to the ocean bottom within the BML, ν ($\sim 1.3 \times 10^{-6}$ m^2 s^{-1}) is the kinematic viscosity and κ_θ ($\sim 1.4 \times 10^{-7}$ m^2 s^{-1}) is the molecular thermal diffusivity. The calculated range for Ra falls between 10^9 and 10^{11}, comparable to values observed in laboratory and numerical experiments (Zhou, Sun & Xia 2007; Ching 2014).

The BML temperature data are separated into two categories, unstable stratification and weak stratification, and the corresponding temperature spectrum of each state is computed. As shown in figure 5(*c*), the unstably stratified convection phase deviates significantly from the BO scaling of $-7/5$. Instead, the best-fitting result yields $\alpha = -1.76 \pm 0.10$, which is closer to the classical scaling of $-5/3$ observed in isotropic turbulence. Previous studies in the atmospheric surface layer have argued that flow dynamics is dominated by both mechanical turbulence and convection under the unstable condition of $-0.03 < Ri < 0$ (Schnelle & Dey 1999). During the observed unstable convection phases, Ri is approximately -3.6×10^{-5} (see figure 5*b*), suggesting the possible significant contribution of turbulent shear too. During the rest of the time, the BML water exhibits a weakly stratified condition with a buoyancy frequency of $N \sim 0.0018$ rad s^{-1}. In these

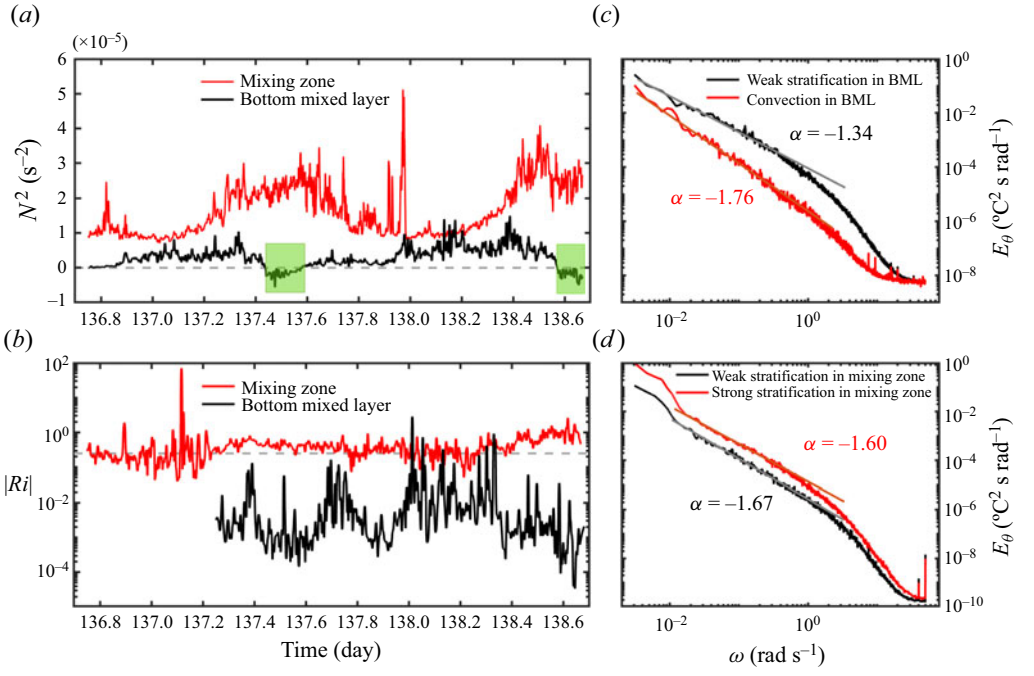

Figure 5. The nominal (*a*) buoyancy frequency squared, N^2, and (*b*) Richardson number, *Ri*, in the mixing zone ($Dab = [10, 40]$ m, red) and BML ($Dab = [0, H_{BML}]$, black). In (*a*), instances of unstable stratified convection are marked with green shading. In (*b*), the grey dashed line at $Ri = 0.25$ is for reference. (*c*) Temperature power spectra in the BML during the convection (red) and weak-stratification (black) phases, with the corresponding fitted scaling exponents of -1.76 and -1.34. (*d*) Temperature power spectra in the mixing zone during weak (black) and strong (red) stratifications, with the corresponding fitted scaling exponents of -1.67 and -1.60.

phases, the scaling $\alpha = -1.34 \pm 0.10$ appears to follow the BO scaling rather than the Kolmogorov scaling.

Recent numerical simulation studies have suggested that the BO scaling occurs in moderately stratified conditions but not in near-neutral or very stable conditions (Kumar *et al.* 2014; Verma *et al.* 2017; Alam *et al.* 2019). Turning our attention back to the mixing zone, as shown in figure 3(*b*), temporal variations in stratification are exhibited. During day [136.75, 137.17] and day [137.79, 138.22], the stratification is weak with N being approximately 0.0024 rad s^{-1}, and the fitted scaling $\alpha = -1.67 \pm 0.05$ is observed in the temperature spectrum (figure 5*d*). In the remaining time, the water exhibits relatively strong stability with an N of 0.0047 rad s^{-1}, and the scaling α is fitted as -1.60 ± 0.10 in the temperature spectrum. Notably, both the scalings are close to the Kolmogorov value of $-5/3$ rather than the BO scaling of $-7/5$.

The above results show that the scaling α follows the BO-like scaling only in the case of weak stratification in the BML ($N \sim 0.0018$ rad s^{-1}). However, in the tightly closed weak stratification of the mixing zone ($N \sim 0.0031$ rad s^{-1}), the scaling adheres to the Kolmogorov-like scaling. This implies the presence of other forces at play. To gain further insights, the Richardson number *Ri* is utilized, which characterizes the interplay between buoyant and shear forces in turbulent conditions. Since the LADCP cannot effectively measure the bottom current close to the seafloor, velocity data from the SeaGuard current meter at $Dab = 2.2$ m were used to estimate the current shear and *Ri* within the BML,

assuming a no-slip boundary condition. As shown in figure 5(*b*), *Ri* exhibits remarkable fluctuations in the BML. In the weakly stratified BML, $Ri \sim 0.0027$ is found, which is approximately two orders of magnitude smaller than the value ($Ri \sim 0.19$) in the mixing zone. This result might imply that the BML is in a more turbulent state and the combination of weak stratification and strong shear promotes a cascade scaling close to that of BO theory. In recent large-eddy simulations of stratified turbulence, it has been found that the BO theory is valid in moderate stratification at $Ri \sim 10$, while the Kolmogorov scaling is followed in strong stratification at $Ri \sim 25$ (Agrawal & Chandy 2021). However, in other high-resolution direct numerical simulations (Kumar *et al.* 2014; Alam *et al.* 2019), it is reported that BO scaling is valid for $Ri \sim 1$ but Kolmogorov scaling is valid for $Ri = 4 \times 10^{-7}$. In these simulations, N typically remains constant and is set to unity. It is essential to exercise caution when comparing these numerical results with the current observations. Basu & Bhattacharjee (2019) also pointed out that N is an important control parameter for producing different scaling regimes. The current results suggest that both stratification and turbulent intensity are key factors in buoyancy-driven turbulent scaling behaviours, providing insights for future study.

5. Conclusions

In summary, we examine the turbulent cascade scalings in the bottom ocean using high-resolution temperature data from a mooring in the northern SCS. The bottom water exhibits three distinct structures in terms of stratification variability, which are classified as the BML, the mixing zone and the internal wave zone with increasing distance from the seafloor. In the weak stratification phase of the BML, a scaling of -1.34 ± 0.10 is observed, which is close to the prediction of the BO theory. The similar cascading behaviours in the oceanic bottom boundary layer and the atmospheric surface layer might suggest common underlying mechanisms driving turbulent states, which merits further study. However, in the unstably stratified convective turbulence within the BML, the scaling of -1.76 ± 0.10 deviates from the BO theory and appears closer to the classical scaling of $-5/3$ in isotropic turbulence, suggesting that the convective turbulence is not the promise of BO scaling. In the mixing zone, the water remains in weakly stable stratification, although it exhibits alternating weak and strong stratification in the diurnal cycle. The scaling is observed to be closer to the Kolmogorov scaling of $-5/3$. The Richardson number in the mixing zone is around 0.25, which is approximately two orders of magnitude larger than that in the BML. Under similar weak stratifications, the scaling comparison in the BML and the mixing zone suggests that strong shear flow promotes the occurrence of BO-like scaling, while weak shear leads to Kolmogorov-like scaling. In the internal wave zone, the more stable stratification is significantly modulated by the intense internal waves. A scaling of 2.12 ± 0.15 is observed in the frequency range higher than the averaged buoyancy frequency N within this region ($\omega > N$). Although the -2 scaling has been extensively observed in the internal wave frequency range ($\omega < N$), the present observation of turbulent states requires further clarification, despite the suggested possible mechanisms as continuously breaking internal waves (Phillips 1971) and chaos theory of Brownian noise (Schuster & Just 2006).

Acknowledgements. Those who helped to collect, calibrate, process and archive the GEBCO grid dataset are appreciated. Data were collected onboard R/V Jiageng implementing the open research cruise NORC2018-06 supported by NSFC Shiptime Sharing Project (project number 41749906).

Funding. This work was supported by the National Key Research and Development Program of China (2021YFC3101300), the National Natural Science Foundation of China (NSFC) (42006196, 42206020, 12172369, 42249907, 42449907), the Basic and Applied Basic Research Foundation of Guangdong Province (2021A1515110839), the Hainan Provincial Natural Science Foundation of China (422QN439), the Science and Technology Projects in Guangzhou (2024A04J4049), the State Key Laboratory of Tropical Oceanography, South China Sea Institute of Oceanology, Chinese Academy of Sciences (LTO2219) and the Hubei Provincial Natural Science Foundation of China (2022CFB334).

Declaration of interests. The authors report no conflict of interest.

Data availability statement. The data that support the findings of this study are openly available in Figshare at https://figshare.com/articles/dataset/2020Dongsha_tripod/25149068.

Author ORCIDs.
Peng-Qi Huang https://orcid.org/0000-0001-6619-3528;
Shuang-Xi Guo https://orcid.org/0000-0002-8524-800X;
Sheng-Qi Zhou https://orcid.org/0000-0001-8647-7034.

References

Agrawal, R. & Chandy, A.J. 2021 Large eddy simulations of forced and stably stratified turbulence: evolution, spectra, scaling, structures and shear. *Intl J. Heat Fluid Flow* **89**, 108778.

Ahlers, G., Grossmann, S. & Lohse, D. 2009 Heat transfer and large scale dynamics in turbulent Rayleigh–Bénard convection. *Rev. Mod. Phys.* **81**, 503.

Alam, S., Guha, A. & Verma, M.K. 2019 Revisiting Bolgiano–Obukhov scaling for moderately stably stratified turbulence. *J. Fluid Mech.* **875**, 961–973.

Alexakis, A. & Biferale, L. 2018 Cascades and transitions in turbulent flows. *Phys. Rep.* **767**, 1–101.

Alford, M.H. *et al.* 2015 The formation and fate of internal waves in the south China sea. *Nature* **521** (7550), 65–69.

Basu, A. & Bhattacharjee, J.K. 2019 Kolmogorov or Bolgiano-Obukhov scaling: universal energy spectra in stably stratified turbulent fluids. *Phys. Rev.* E **100** (3), 033117.

Becherer, J. & Moum, J.N. 2017 An efficient scheme for onboard reduction of moored χpod data. *J. Atmos. Ocean. Technol.* **34** (11), 2533–2546.

Bolgiano, R., Jr. 1959 Turbulent spectra in a stably stratified atmosphere. *J. Geophys. Res.* **64** (12), 2226–2229.

Calzavarini, E., Toschi, F. & Tripiccione, R. 2002 Evidences of Bolgiano-Obhukhov scaling in three-dimensional Rayleigh–Benard convection. *Phys. Rev.* E **66**, 016304.

Chiba, O. 1989 Buoyant subrange observed in the stably stratified atmospheric surface layer. *J. Appl. Meteorol. Climatol.* **28** (11), 1236–1243.

Ching, E.S.C. 2014 *Statistics and Scaling in Turbulent Rayleigh–Benard Convection*. Springer.

Chriss, T.M.C. & Caldwell, D.R. 1984 Turbulence spectra from the viscous sublayer and buffer layer at the ocean floor. *J. Fluid Mech.* **142**, 39–55.

Cot, C. & Barat, J. 1989 Spectral analysis of high resolution temperature profiles in the stratosphere. *Geophys. Res. Lett.* **16** (10), 1165–1168.

Ewart, T.E. 1976 Observations from straightline isobaric runs of SPURV. In *Proc. IAPSO/IAMAP PSII, Edinburgh, UK*, pp. 1–18. Joint Oceanographic Assembly.

Frehlich, R. & Sharman, R. 2010 Climatology of velocity and temperature turbulence statistics determined from rawinsonde and ACARS/AMDAR data. *J. Appl. Meteorol. Climatol.* **49** (6), 1149–1169.

Frisch, U. 1995 *Turbulence: The Legacy of A.N. Kolmogorov*. Cambridge University Press.

Gage, K.S. 1985 A climatology of atmospheric wavenumber spectra of wind and temperature observed by commercial aircraft. *J. Atmos. Sci.* **42**, 950–960.

Ganachaud, A. & Wunsch, C. 2000 Improved estimates of global ocean circulation, heat transport and mixing from hydrographic data. *Nature* **408** (6811), 453–457.

Gargett, A.E., Hendricks, P.J., Sanford, T.B., Osborn, T.R. & Williams, A.J. 1981 A composite spectrum of vertical shear in the upper ocean. *J. Phys. Oceanogr.* **11** (9), 1258–1271.

Gargett, A.E., Osborn, T.R. & Nasmyth, P.W. 1984 Local isotropy and the decay of turbulence in a stratified fluid. *J. Fluid Mech.* **144**, 231–280.

Garrett, C. & Munk, W. 1972 Space-time scales of internal waves. *Geophys. Astrophys. Fluid Dyn.* **3** (1), 225–264.

GREGG, M.C. 1977 Variations in the intensity of small-scale mixing in the main thermocline. *J. Phys. Oceanogr.* **7**, 436–454.

GROSS, T.F. & NOWELL, A.R.M. 1985 Spectral scaling in a tidal boundary layer. *J. Phys. Oceanogr.* **15** (5), 496–508.

VAN HAREN, H. 2022 KMT, kilometer-long mooring of high-resolution temperature measurements results overview. *Dyn. Atmos. Oceans* **100**, 101336.

VAN HAREN, H. 2023 Convection and intermittency noise in water temperature near a deep Mediterranean seafloor. *Phys. Fluids* **35** (2), 026604.

VAN HAREN, H. & BOSVELD, F. 2022 Internal wave and turbulence observations with very high-resolution temperature sensors along the Cabauw mast. *J. Atmos. Ocean. Technol.* **39**, 1149–1165.

VAN HAREN, H. & DIJKSTRA, H.A. 2021 Convection under internal waves in an alpine lake. *Environ. Fluid Mech.* **21**, 305–316.

VAN HAREN, H. & GOSTIAUX, L. 2009 High-resolution open-ocean temperature spectra. *J. Geophys. Res.* **114** (C5), C05005.

VAN HAREN, H., VOET, G., ALFORD, M.H., FERNÁNDEZ-CASTRO, B., NAVEIRA GARABATO, A.C., WYNNE-CATTANACH, B.L., MERCIER, H. & MESSIAS, M.-J. 2024 Near-slope turbulence in a Rockall canyon. *Deep-Sea Res. I* **206**, 104277.

HIERONYMUS, M., NYCANDER, J., NILSSON, J., DÖÖS, K. & HALLBERG, R. 2019 Oceanic overturning and heat transport: the role of background diffusivity. *J. Clim.* **32** (3), 701–716.

HOLBROOK, W.S. & FER, I. 2005 Ocean internal wave spectra inferred from seismic reflection transects. *Geophys. Res. Lett.* **32** (15), L15604.

HUANG, P.-Q., CEN, X.-R., GUO, S.-X., LU, Y.-Z., ZHOU, S.-Q., QIU, X.-L., ZHANG, J.-Z., WU, Z.-L. & HAN, G.-H. 2021 Variance of bottom water temperature at the continental margin of the northern south China sea. *J. Geophys. Res.* **126** (2), e2020JC015843.

HUANG, P.-Q., CEN, X.-R., LU, Y.-Z., GUO, S.-X. & ZHOU, S.-Q. 2019 Global distribution of the oceanic bottom mixed layer thickness. *Geophys. Res. Lett.* **46** (3), 1547–1554.

KERR, R.M. 1996 Rayleigh number scaling in numerical convection. *J. Fluid Mech.* **310**, 139–179.

KLYMAK, J.M. & MOUM, J.N. 2007 Oceanic isopycnal slope spectra. Part 2. Turbulence. *J. Phys. Oceanogr.* **37** (5), 1232–1245.

KOLMOGOROV, A.N. 1941 The local structure of turbulence in incompressible viscous fluid for very large Reynolds number. *Dokl. Akad. Nauk SSSR* **30**, 301–303.

KUMAR, A., CHATTERJEE, A.G. & VERMA, M.K. 2014 Energy spectrum of buoyancy-driven turbulence. *Phys. Rev.* E **90** (2), 023016.

KUNNEN, R., CLERCX, H., GEURTS, B., BOKHOVEN, L. & AKKERMANS, R.A.D. 2008 Numerical and experimental investigation of structure-function scaling in turbulent Rayleigh–Benard convection. *Phys. Rev.* E **77**, 016302.

LAZAREV, A., SCHERTZER, D., LOVEJOY, S. & CHIGIRINSKAYA, Y. 1994 Unified multifractal atmospheric dynamics tested in the tropics. Part 2. Vertical scaling and generalized scale invariance. *Nonlinear Process. Geophys.* **1** (2/3), 115–123.

LIEN, R.-C. & SANFORD, T.B. 2004 Turbulence spectra and local similarity scaling in a strongly stratified oceanic bottom boundary layer. *Cont. Shelf Res.* **24** (3), 375–392.

LOHSE, D. & XIA, K.-Q. 2010 Small-scale properties of turbulent Rayleigh–Bénard convection. *Annu. Rev. Fluid Mech.* **42**, 335–364.

LUMLEY, J.L. 1964 The spectrum of nearly inertial turbulence in a stably stratified fluid. *J. Atmos. Sci.* **21** (1), 99–102.

MEREDITH, M. & GARABATO, A.N. 2021 *Ocean Mixing: Drivers, Mechanisms and Impacts*. Elsevier.

MONIN, A.S. 1962 On the turbulence spectrum in a thermally stratified atmosphere. *Bull. Acad. Sci. USSR Ser. Geophys.* **3**, 266–271.

MOUM, J.N. 2015 Ocean speed and turbulence measurements using pitot-static tubes on moorings. *J. Atmos. Ocean. Technol.* **32** (7), 1400–1413.

MYRUP, L.O. 1969 Turbulence spectra in stable and convective layers in the free atmosphere. *Tellus* **21** (3), 341–354.

OBUKHOV, A. 1959 Effect of archimedean forces on the structure of the temperature field in a turbulent flow. *Dokl. Akad. Nauk SSSR* **125**, 1246–1248.

OKAMOTO, M. & WEBB, E.K. 1970 The temperature fluctuations in stable stratification. *Q. J. R. Meteorol. Soc.* **96** (410), 591–600.

OSBORN, T.R. 1980 Estimates of the local rate of vertical diffusion from dissipation measurements. *J. Phys. Oceanogr.* **10** (1), 83–89.

PHILLIPS, O.M. 1971 On spectra measured in an undulating layered medium. *J. Phys. Oceanogr.* **1** (1), 1–6.

POLZIN, K., WANG, B., WANG, Z., THWAITES, F. & WILLIAMS, A. 2021 Moored flux and dissipation estimates from the northern deepwater gulf of Mexico. *Fluids* **6**, 237.

QU, L. *et al.* 2021 Temporal variability in bottom water structures of the continental slope in the northern South China Sea. *J. Geophys. Res.* **126** (7), e2021JC017177.

SCHNELLE, K.B. & DEY, P.R. 1999 *Atmospheric Dispersion Modeling Compliance Guide*. McGraw-Hill.

SCHUSTER, H.G. & JUST, W. 2006 *Deterministic Chaos: An Introduction*. John Wiley & Sons.

SHESTAKOV, A.V., STEPANOV, R.A. & FRICK, P.G. 2017 On cascade energy transfer in convective turbulence. *J. Appl. Mech. Tech. Phys.* **58**, 1171–1180.

SHIMIZU, K. 2010 An analytical model of capped turbulent oscillatory bottom boundary layers. *J. Geophys. Res.* **115** (C3), C03011.

ST. LAURENT, L., SIMMONS, H., TANG, T.Y. & WANG, Y. 2011 Turbulent properties of internal waves in the South China Sea. *Oceanography* **24** (4), 78–87.

TIAN, J., YANG, Q. & ZHAO, W. 2009 Enhanced diapycnal mixing in the South China Sea. *J. Phys. Oceanogr.* **39** (12), 3191–3203.

TROWBRIDGE, J.H. & LENTZ, S.J. 2018 The bottom boundary layer. *Annu. Rev. Mar. Sci.* **10** (1), 397–420.

VERMA, M.K., KUMAR, A. & PANDEY, A. 2017 Phenomenology of buoyancy-driven turbulence: recent results. *New J. Phys.* **19** (2), 025012.

WEATHERLY, G.L. & MARTIN, P.J. 1978 On the structure and dynamics of the oceanic bottom boundary layer. *J. Phys. Oceanogr.* **8** (4), 557–570.

WERNE, J. & FRITTS, D.C. 2000 Structure functions in stratified shear turbulence. In *10th DoD HPC User Group Conference, Albuquerque, NM*. Department of Defense, USA.

WROBLEWSKI, D.E., COTE, O.R., HACKER, J.M. & DOBOSY, R.J. 2010 Velocity and temperature structure functions in the upper troposphere and lower stratosphere from high-resolution aircraft measurements. *J. Atmos. Sci.* **67**, 1157–1170.

WROBLEWSKI, D.E., COTE, O.R., HACKER, J.M. & DOBOSY, R.J. 2007 Cliff–ramp patterns and Kelvin–Helmholtz billows in stably stratified shear flow in the upper troposphere: analysis of aircraft measurements. *J. Atmos. Sci.* **64** (7), 2521–2539.

WU, X.Z., KADANOFF, L., LIBCHABER, A. & SANO, M. 1990 Frequency power spectrum of temperature fluctuations in free convection. *Phys. Rev. Lett.* **64**, 2140.

WUNSCH, C. & FERRARI, R. 2004 Vertical mixing, energy, and the general circulation of the ocean. *Annu. Rev. Fluid Mech.* **36**, 281–314.

YAKHOT, V. 1992 4/5 Kolmogorov law for statistically stationary turbulence: application to high Rayleigh number Bénard convection. *Phys. Rev. Lett.* **69**, 769.

YANG, Q., ZHAO, W., LIANG, X. & TIAN, J. 2016 Three-dimensional distribution of turbulent mixing in the South China Sea. *J. Phys. Oceanogr.* **46** (3), 769–788.

ZHAO, Z. 2014 Internal tide radiation from the Luzon Strait. *J. Geophys. Res.* **119** (8), 5434–5448.

ZHOU, S.-Q., SUN, C. & XIA, K.-Q. 2007 Measured oscillations of the velocity and temperature fields in turbulent Rayleigh–Bénard convection in a rectangular cell. *Phys. Rev.* E **76**, 036301.

ZHOU, S.-Q. & XIA, K.-Q. 2001 Scaling properties of the temperature field in convective turbulence. *Phys. Rev. Lett.* **87**, 064501.